

Diuary Gonçalves

**Impedance Modeling and Analysis of
Distributed Generation Grid-Tie Inverters**

Viçosa, MG

2022

Diuary Gonçalves

Impedance Modeling and Analysis of Distributed Generation Grid-Tie Inverters

Monograph presented to the Department of Electrical Engineering of the Exact Sciences Center of the Federal University of Viçosa, in order to obtain the credits of the ELT 402 subject - Projeto de Engenharia II - and fulfillment of the partial requirement to obtain the Bachelor's degree in Electrical Engineering.

Supervisor: Heverton Augusto Pereira
Co-Supervisor: João Victor Matos Farias

Viçosa, MG

2022

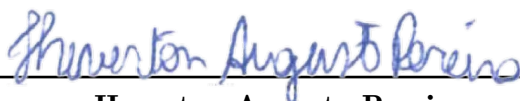
Diuary Gonçalves

Impedance Modeling and Analysis of Distributed Generation Grid-Tie Inverters

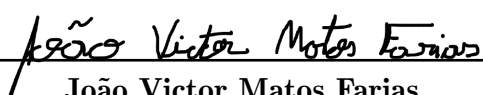
Monograph presented to the Department of Electrical Engineering of the Exact Sciences Center of the Federal University of Viçosa, in order to obtain the credits of the ELT 402 subject - Projeto de Engenharia II - and fulfillment of the partial requirement to obtain the Bachelor's degree in Electrical Engineering.

Work approved in 2022 february 11.

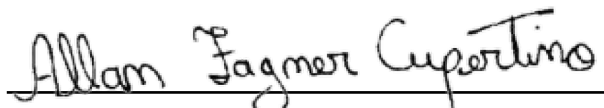
EXAMINATING COMMITTEE



Heverton Augusto Pereira
Supervisor



João Victor Matos Farias
Co-Supervisor



Allan Fagner Cupertino
Evaluator Member



Renata Oliveira de Sousa
Evaluator Member

Viçosa, MG

2022

Agradecimentos

I would like to express my special thanks to my family, that support me during all my graduation and allowed me to have such a good experience.

Also to my advisors Heverton Augusto Pereira and João Victor Matos Faria, who contributed directly to the production of this work.

My thanks to the research group GESEP¹.

Special acknowledgements to the Department of Electrical Engineering at Universidade Federal de Viçosa².

And finally, to all my friends, that together walked the same path, aiding one another.

¹ Gerência de Especialistas em Sistemas Elétricos de Potência, that allowed my improvement. <<https://www.gesep.ufv.br/>>

² <<https://del.ufv.br/>>

*“The greatest enemy of knowledge is not ignorance,
it is the illusion of knowledge” (Stephen W. Hawking)*

Resumo

Nos últimos anos, ocorreu um aumento no número de sistemas baseados em eletrônica de potência conectados à rede. Isso ocorre principalmente devido ao crescente número de geração fotovoltaica, os quais podem trazer problemas de instabilidade para a rede elétrica. Dessa maneira, diferentes modelos para representar inversores conectados a rede são apresentados na literatura, um dos mais utilizados o modelo equivalente de Norton. Nesse trabalho, uma nova estratégia é apresentada para modelar o sistema fotovoltaico como componentes passivos. O sistema é baseado no modelo médio de um inversor, em que a impedância de saída é obtida através da regra de Mason aplicada no diagrama de blocos. Para cada frequência harmônica representada no sistema, um circuito de análise extra é necessário. Diferentes categorias de controle foram implementados para avaliar o modelo proposto em sua precisão e generalidade. Algumas mudanças no sistema envolvem a corrente utilizada na realimentação do sistema, estratégias de amortecimento e controle. A distorção total de demanda é utilizada como método de comparação entre o modelo chaveado convencional e o modelo proposto, o modelo proposto consegue obter um erro relativo inferior a 1%. Além disso, uma análise do tempo de simulação de cada modelo é realizada, em que o modelo chaveado apresenta tempos de simulação entre 18 s e 23 s, enquanto o modelo proposto apresenta tempos entre 0.28 s e 0.33 s.

Palavras-chave: Redes distribuídas, distorção, interação harmônica, inversores, modelo de Norton.

Abstract

In recent years, an increase in the number of grid connected power electronics-based systems. This is mainly due to the increase of photovoltaics system generation, which significantly increase stability concerns to the electrical grid. Therefore, different models to represent the inverter-grid interaction are presented in the literature. The most used is the Norton equivalent-based model. This work proposes a new strategy to model the photovoltaic inverter through passive components. The system is based in the average model of the inverter, where the output impedance is obtained through the Mason's rule. For each frequency of interest, a different passive circuit is needed. Different types of control are implemented to evaluate the proposed model generality and accuracy. Some changes are the current feedback, the damping strategy and control strategy. A comparison between the Total Demand Distortion of a convectional switching, where the proposed model presented a relative error below 1%. Besides, an analysis of the time performance of each model is performed, where the switching model has a simulation time between 18 s and 23 s, as for the proposed model the time is between 0.28 s and 0.33 s.

keywords: Distributed generation, distortion, harmonic interactions, inverters, Norton modeling.

List of Figures

Figura 1 – Main aspects of VSC control (Jacinto, 2021).	14
Figura 2 – General diagram of the switching model of a three-phase DG inverter.	16
Figura 3 – General diagram of the average model of the inverter considering (a) grid current (i_g) feedback and (b) inverter current feedback (i_f).	16
Figura 4 – Norton Equivalent model of a grid connected inverter.	17
Figura 5 – RLC circuit related to each harmonic order n in analysis.	19
Figura 6 – Diagram of the average model for the system with PD for the: (a) grid current feedback and (b) converter current feedback. The resistor implementation is represented in red.	20
Figura 7 – Diagram of the average model for the system with CCF for the: (a) grid current feedback and (b) converter current feedback. The feedback implementation is represented in red.	21
Figura 8 – Diagram of the average model for the system with CVF for the: (a) grid current feedback and (b) converter current feedback. The feedback with the filter implementation is represented in red.	22
Figura 9 – Diagram of the average model for the system with NF for the: (a) grid current feedback and (b) converter current feedback. The notch filter implementation is indicated in red.	23
Figura 10 – Grid voltage source behavior	26
Figura 11 – Bode diagram, comparison of the output impedance of the transfer function and the Norton model for a specific frequency.	27
Figura 12 – Bode diagram of the output impedance for the model in DQ, where Z_o is the impedance without frequency shifting, Z_o+ the impedance for the positive sequence and Z_o- for the negative.	28
Figura 13 – Graph in time with the grid current response for the switching and proposed model, and theirs spectrum response with zoom in the harmonics.	29
Figura 14 – Graph in time with the grid current response for the switching and proposed model, and theirs spectrum response with zoom in the harmonics. The results of the switching model are presented for the SRF and DSOGI PLL	29
Figura 15 – Graph indicating the behavior of the TDD error and simulation time in different step size for each model.	31

Lista de tabelas

Tabela 1 – Inverter and grid parameters employed in the simulations.	25
Tabela 2 – Damp values of each strategy employed.	25
Tabela 3 – Percentage value of each voltage harmonic presented in the grid.	26
Tabela 4 – Values of TDD for each of the implementation for the control in the DQ frame.	30
Tabela 5 – Values of TDD for each of the implementation for the control in the $\alpha\beta$ frame.	30
Tabela 6 – Average time each simulation took with 5 samples in the $\alpha\beta$ frame. . .	31
Tabela 7 – Average time each simulation took with 5 samples in the DQ frame. . .	32

Lista de abreviaturas e siglas

BESS	Battery Energy Storage Systems
CCF	Capacitor Current Feedback
CVF	Capacitor Voltage Feedback
DG	Distributed Generation
DSOGI	Dual Second Order Generalized Integrator - Phase Locked Loop
HVDC	High-Voltage Direct Current
LCCs	Line-Commutated Converters
NF	Notch Filter
SCR	Short-Circuit Ratio
SRF	Synchronous Reference Frame
TDD	Total Demand Distortion
PCC	Point of Common Coupling
PD	Passive Damping
PI	Proportional Integral
PR	Proportional Resonant
PLL	Phase-locked Loop
PV	Photovoltaic
VSCs	Voltage-Source Converters
WPPs	Wind Power Plants

Lista de símbolos

C	Filter capacitance
f_n	Rated Frequency
f_{sw}	Switching frequency
G_c	Control transfer function
G_d	Delay transfer function
i_f	Inverter-side current
i_g	Grid-side current
i_o	Inverter reference current
K_i	Integral gain
K_p	Proportional gain
K_r	Resonant gain
L_f	Filter inductance - inverter side
L_g	Filter inductance - grid side
L_{gg}	Grid inductance
n	Harmonic order
P_n	Rated Power
R	Z_o real part
v_o	PCC voltage
V_{dc}	dc-link voltage
V_l	Rated line-to-line Voltage
X	Z_o imaginary part
Z_c	Filter capacitor impedance
Z_f	Converter-side filter inductor impedance
Z_g	Grid-side filter inductor impedance
Z_o	Inverter output impedance

Sumário

1	INTRODUCTION	12
1.1	Motivation	12
1.2	Objectives and Contributions	13
1.3	Sectioning	13
2	SYSTEM DESCRIPTION	14
2.1	Grid-Tied Three-Phase DG Inverter Models	14
2.2	Three-Phase DG Inverter Switching Model	15
2.3	Three-Phase DG Inverter Average Model	15
2.4	Three-Phase DG Inverter Norton Model	17
2.5	Proposed Impedance-Based Norton Model	17
2.6	Damping strategies in the average model	19
2.6.1	Passive damping	19
2.6.2	Capacitor Current Feedback	20
2.6.3	Capacitor Voltage Feedback	21
2.6.4	Notch Filter	22
2.6.5	Control transfer function for the DQ and $\alpha\beta$ frames	23
3	CASE STUDY	25
4	RESULTS AND DISCUSSIONS	27
5	CONCLUSION	33
	REFERÊNCIAS	34

1 Introduction

Modern power grid systems are migrating from standard electrical machines generation systems to power electronic-based power systems (Wang; Blaabjerg, 2019). The renewable energy and Distributed Generation (DG) resources, such as photovoltaic (PV) and wind power plants (WPPs), as an important alternative to conventional generation structures (Puranik; Zhang; Qin, 2018). Allied to the increasing penetration of renewable energy resources, battery energy storage systems (BESS) need to be integrated in the power systems to compensate power fluctuations due to intermittent resources (Puranik; Zhang; Qin, 2018). With the recent popularization of electric vehicles, battery market has massively expanded (Gao et al., 2020). Therefore, the energy storage systems of these vehicles can also be used to compose the energy storage station for the power grid, working similarly to a BESS. These changes will lead to modern power grids with high flexibility, sustainability and improved efficiency (Wang; Blaabjerg, 2019). Under such conditions, the use of power converters in grid-tie applications is stimulated due to the energy generation profile of these sources, requiring a BESS to provide energy in low power moments. Thus, a massive increase of grid-tie inverters is expected in the next years (Cespedes; Sun, 2014).

1.1 Motivation

A numerous amount of inverters connected to the grid are known to cause harmonic interactions between the distribution grid and the inverter. Distorted grid voltages lead to inverter current to become distorted as well, which aggravate the total distortion of the grid voltage by introducing harmonics in the distributed system (Wang et al., 2011). Some works evaluate the abnormal harmonics and resonances in power systems caused by power electronics (Mollerstedt; Bernhardsson, 2000; Vieto; Sun, 2015; Li, 2018). In wind power plants, depending on the impedance characteristics of the plant and the grid, a resonance effect can occur below or above the synchronous frequency of the grid (Vieto; Sun, 2015). Conventional filters may not mitigate the problems effectively due to the frequencies of the instabilities vary in large scale (Li, 2018). Incidents have been reported with the grid integration of high-speed trains. The locomotives use high-frequency converters to improve performance and reduce losses. However, these converters can interact with each other via main grid, causing unpredicted instability problems (Mollerstedt; Bernhardsson, 2000).

Previous works have already discussed and modeled ways to analyze these harmonic interactions through inverter output impedance. This impedance is influenced by the inverter topology and the control strategy utilized (Heskens; Duarte, 2007). An interesting approach to the analysis of this problem is using the impedance of the grid and the inverter

to formulate the small-signal stability using the Nyquist stability criterion (Puranik; Zhang; Qin, 2018). Where the inverter is modeled by the Norton equivalent impedance and the Thévenin equivalent impedance is applied to the power grid. Recent approaches have tried to incorporate the Phase-Locked Loop (PLL) effect in the Norton equivalent model (Wang et al., 2018), although there is an associated difficulty to represent it using passive elements, due to the PLL active characteristic in low frequency bands.

1.2 Objectives and Contributions

The objective of this work is to develop a model representation of a Grid-Tie inverter. This representation consider the inverter behavior as a Norton circuit. The parallel impedance is obtained through the output impedance of the inverter. For each of the harmonic frequencies represented, a different Norton circuit is required. The inverter output impedance is represented by an RLC circuit.

The proposed model does not have a control loop and semiconductor in the system. Therefore, simplifying the circuit, although maintaining its accuracy. As the proposed circuit does not directly represent any control loops, and disregards the switching, it is possible to simulate the system in a higher step size, diminishing the simulation time.

1.3 Sectioning

This work is divided in five chapters. The first chapter introduces the motivation, objectives and contribution. The second chapter presents the system composed of the Grid-Tie inverter and the proposed model development and considerations. The third chapter presents the case study. The fourth chapter discusses the results with a comparison between the proposed and switching model. The fifth chapter is the final considerations and conclusion.

2 System description

2.1 Grid-Tied Three-Phase DG Inverter Models

The harmonic stability problem is not a recent issue, and it was earlier reported in the commissioning stage of the High Voltage Direct Current (HVDC) Cross-Channel link in 1961 (Wang; Blaabjerg, 2019). This HVDC system was based on the Line-Commutated Converters (LCCs), where the voltage distortion caused by a high grid impedance, i.e. a low Short-Circuit Ratio (SCR) grid. This leads to asymmetric firing angles for the LCC, which consequently distorts the grid current with the unexpected harmonics, and forms a positive feedback loop with the grid impedance (Wang; Blaabjerg, 2019). Voltage-Source Converters (VSCs) are dominantly found in the present power electronic based power systems, traction power networks, and microgrids. In these systems, the harmonic stability have different forms, due to the multiple timescale control dynamics of VSCs (Wang; Blaabjerg, 2019).

Therefore, this section discusses models for the grid-tie inverter harmonic analysis. Furthermore, the main aspects of the VSC control approached in this work are highlighted in Figure 1.

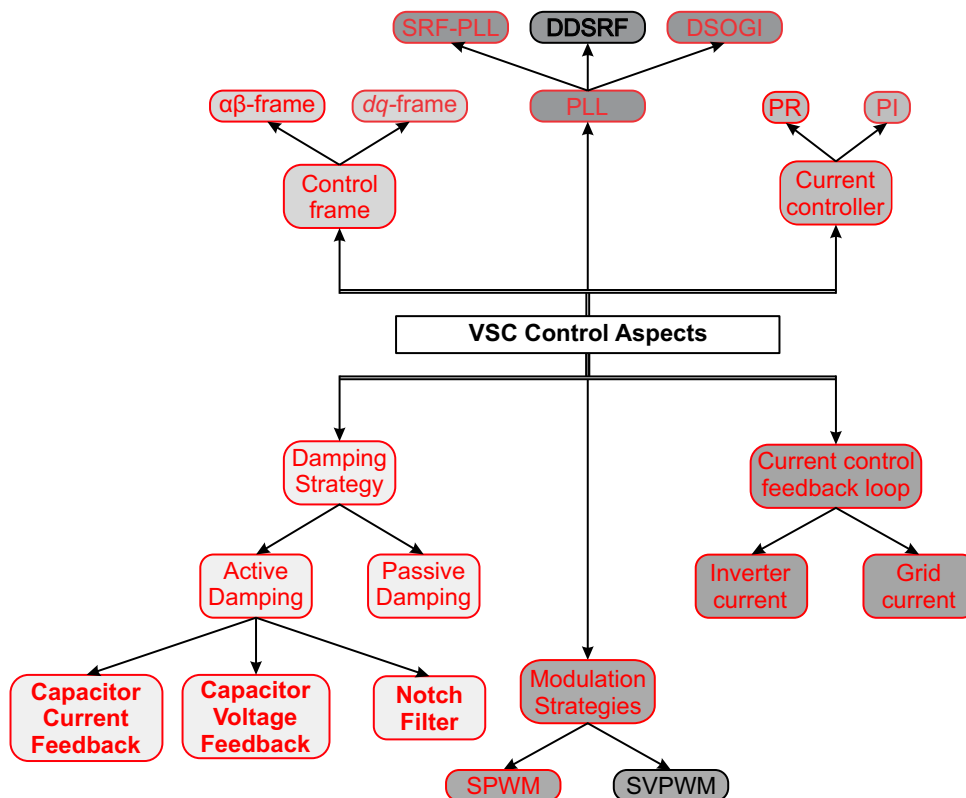


Figura 1 – Main aspects of VSC control (Jacinto, 2021).

The red-dotted blocks in the diagram indicates the aspects that are varied in the VSC control structure, as listed:

1. Current control feedback loop: whether the inverter-side current (i_f) is used, or the grid-side current (i_g);
2. Reference frame transformation: the VSC control is realized in the $\alpha\beta$ -frame or in the dq -frame;
3. Damping strategy: Passive damping (PD) using damping resistor (R_d), or the use of one of the following active damping (AD) strategies, capacitor current feedback (CCF), capacitor voltage feedback (CVF) and Notch filter (NF);
4. Phase locked loop: The use of the Dual Second Order Generalized Integrator - PLL (DSOGI-PLL) or the Synchronous Reference Frame - PLL (SRF-PLL) structure when the control is made in the DQ-frame;
5. Current controller: A proportional resonant (PR) controller is implemented when considering $\alpha\beta$ -frame control, or the use of a proportional integral (PI) controller when considering DQ-frame.

2.2 Three-Phase DG Inverter Switching Model

Figure 2 illustrates a general schematic, the switching model of the VSC. As observed, the inverter is coupled to the grid by an LCL filter at the point of common coupling (PCC). The grid is represented by a Thévenin model, with a voltage source (v_{th}) and impedance (Z_{th}). The DC-link is considered controlled and constant, and is modelled as a constant voltage source. In this sense, the VSC control is done in a single stage conversion structure. Moreover, only the current control loop is considered in this model. ρ is the PLL phase output.

The switching model is used as basis, since it represents to depict all the electrical dynamics of the VSC, from the switching of the semiconductor devices, to the resonant frequency of the LCL filter. Therefore, it is a more accurate model for representation of the VSC.

2.3 Three-Phase DG Inverter Average Model

This model represents the VSC current control loop in the form of a block diagram, as Fig. 3 illustrates. Notice that in Fig.3(a), the diagram represents the VSC control when considering grid current (i_g) feedback, while Fig. 3(b) illustrates the case of inverter current

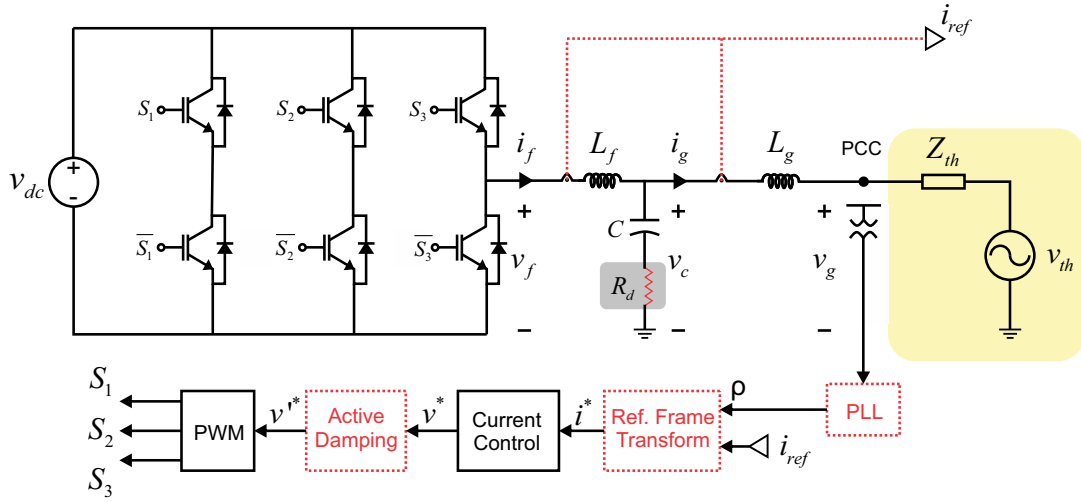


Figura 2 – General diagram of the switching model of a three-phase DG inverter.

(i_f) feedback. The varying aspects of the control, as listed in the previous subsection, are highlighted by red-dotted lines.

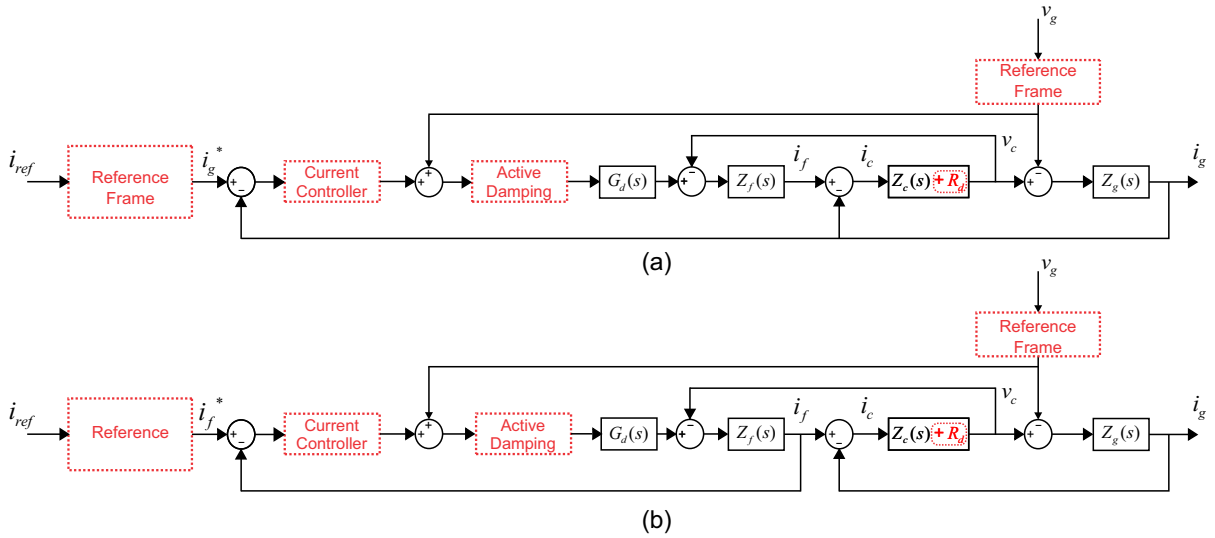


Figura 3 – General diagram of the average model of the inverter considering (a) grid current (i_g) feedback and (b) inverter current feedback (i_f).

The average model is of utmost importance for the proposed Norton model, not as a mean of comparison, but for the obtainment the inverter output impedance $Z_o(s)$, which in this case was obtained by applying Mason Gain Formula to the block diagram.

2.4 Three-Phase DG Inverter Norton Model

A single-phase inverter system is used to interpret harmonic interaction problems, although it also represents typically one phase of a three-phase inverter (Wang et al., 2011). To describe a general case, all the currents at the AC side and the grid voltage are assumed to be measured, although only the necessary control variables are needed depending on the control strategy. Considering that the control of the dc bus can be achieved by an upstream power conversion stage, or that the dc-bus control has a large time constant with respect to inverter current regulation, only inner loop control is considered (Wang et al., 2011).

Since the DG inverter is controlled to inject current into the grid, the inverter is represented by a Norton model (i.e., a current source i_o and a parallel output impedance Z_o), as shown in Fig. 4. In principle, Norton model and Thevenin model are equivalent for the analysis here; however, it is convenient to represent the inverters in the form of the Norton model, especially for the impedance calculation. The output impedance of an inverter leads to output harmonic currents due to the interaction with the corresponding grid voltage harmonics.

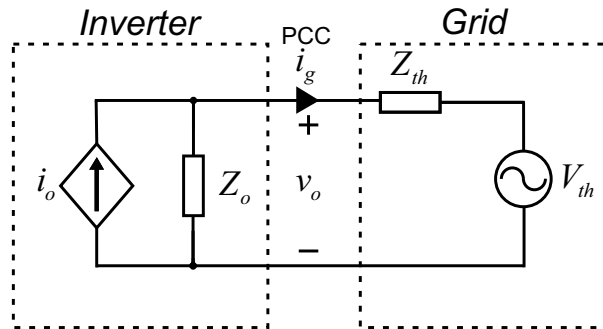


Figura 4 – Norton Equivalent model of a grid connected inverter.

Based on the Norton model of the inverter, where most of the inverter dynamics can be depicted by its output impedance Z_o as a function of the complex frequency, an impedance-based Norton model is proposed in the next section. The proposed model consists of a well-defined RLC circuit for each harmonic in the system, and the parameters of the circuit (R,L and C) depend on the values of $Z_o(s)$ on the harmonic frequency which each circuit represents.

2.5 Proposed Impedance-Based Norton Model

A Norton Model such as the one shown in Fig. 4 can be obtained from the average circuit model by calculating the output impedance Z_o . By analyzing the Norton Equivalent

circuit based on the small-signal analysis around an operation point, the output impedance can be calculated by equation (Puranik; Zhang; Qin, 2018):

$$Z_o(s) = - \left. \frac{v_o(s)}{i_g(s)} \right|_{i_o(s)=0}, \quad (2.1)$$

where v_o is the PCC voltage, i_g is the current flowing to the grid and i_o is the inverter reference current.

Equation (2.1) can be obtained for any inverter represented by the average model. Additionally, since Z_o was obtained in the frequency domain, its value can be calculated for each harmonic order n , as (2.2) indicates. Now, an RLC circuit can be established for each value of n , if the impedance is passive. Figure 5 elucidates how each harmonic is related to an independent RLC circuit. The RLC arrange is the same for all values of n , and it was chosen that way so the inductor current is not forced by the current source, and the capacitor voltage is not forced by the voltage source.

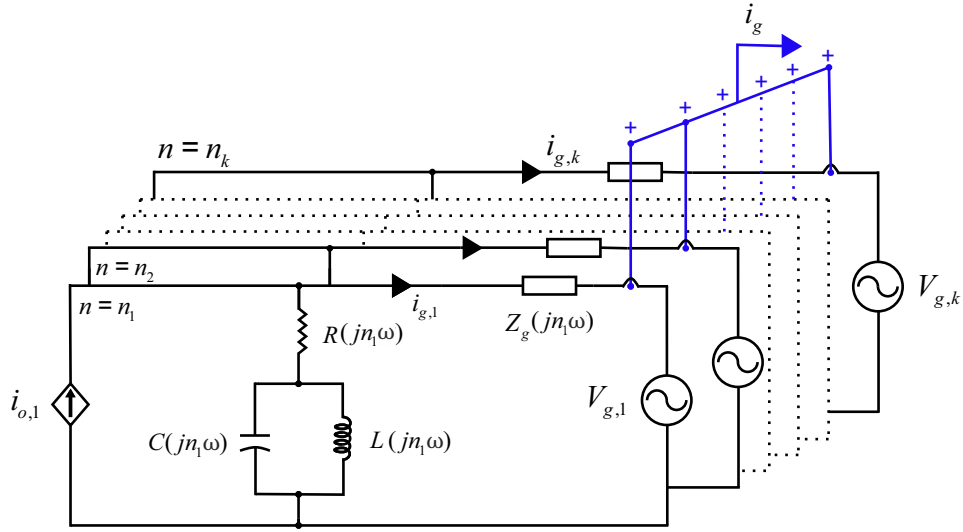
$$Z_o(jn\omega) = R(jn\omega) \pm jX(jn\omega), \quad (2.2)$$

where n is harmonic order and ω is the fundamental angular frequency.

Therefore, the real and imaginary values of (2.2) can be attributed to the passive elements in the RLC circuit. The resistance R receives the real value of $Z_o(jn\omega)$. The inductance and the capacitance in the branch receive different values depending on the imaginary value of $Z_o(jn\omega)$, as indicated in Eqs. (2.3) and (2.4). If $Z_o(jn\omega)$ has capacitive characteristics, i.e. $Im(Z_o) < 0$, only the capacitor should be present in the circuit, so the inductor branch must become an open circuit ($L \rightarrow \infty$). The analysis is similar for inductive characteristics of $Z_o(jn\omega)$.

$$C(jn\omega) = \begin{cases} \frac{1}{n\omega X(jn\omega)}, & Im(Z_o(jn\omega)) < 0 \\ \approx 0, & Im(Z_o(jn\omega)) > 0 \end{cases} \quad (2.3)$$

$$L(jn\omega) = \begin{cases} \rightarrow \infty, & Im(Z_o(jn\omega)) < 0 \\ \frac{X(jn\omega)}{n\omega}, & Im(Z_o(jn\omega)) > 0 \end{cases} \quad (2.4)$$


 Figura 5 – RLC circuit related to each harmonic order n in analysis.

2.6 Damping strategies in the average model

Four different damping strategies are implemented, all strategies are presented in (Gomes; Cupertino; Pereira, 2018), where the methodology of adjust is based on a pole placement. For each strategy, a variable is adjusted for damp factor tuning of 0.15.

2.6.1 Passive damping

The PD introduces a passive component in the LCL filter. In this work a damping resistor is added in series with the filter capacitor, its resistance (R_d) is used for the tuning. Fig. 6 shows the block diagram for the PD with the grid and converter current feedback.

In Fig. 6, Z_f and Z_g are the filter inductor impedance for the converter and grid side, respectively. Z_c is the filter capacitor impedance, G_d the delay transfer function, and G_c the control transfer function, that depends on the implemented strategy and is further discussed. The model of the function are presented as follows:

$$Z_f = sL_f + R_f, \quad (2.5)$$

$$Z_g = sL_g + R_g, \quad (2.6)$$

$$Z_c = \frac{1}{sC}, \quad (2.7)$$

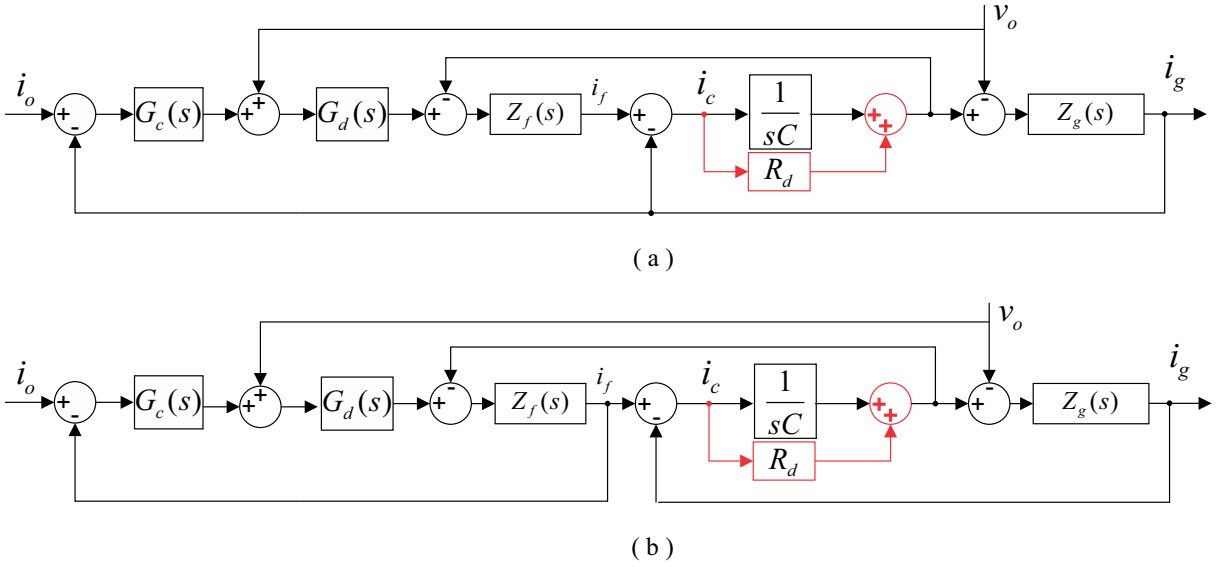


Figura 6 – Diagram of the average model for the system with PD for the: (a) grid current feedback and (b) converter current feedback. The resistor implementation is represented in red.

$$G_d = \frac{1}{1.5T_s s + 1}, \quad (2.8)$$

where L_f is the filter inductance in the converter side, R_f is its resistance. For the filter inductor in the grid side, L_g is the inductance and R_g the resistance. C is the filter capacitor capacitance. T_s is the sampling time. The transfer functions of Z_o for the grid Z_{og} and converter Z_{of} current feedback are:

$$Z_{og}(s) = \frac{Z_f + (Z_c + R_d) - G_d(Z_c + R_d)}{Z_f Z_g + (Z_c + R_d)Z_g + (Z_c + R_d)Z_f + G_c G_d (Z_c + R_d)}, \quad (2.9)$$

$$Z_{of}(s) = \frac{Z_f + (Z_c + R_d) - G_d(Z_c + R_d) + G_c G_d}{Z_f Z_g + (Z_c + R_d)Z_g + (Z_c + R_d)Z_f + G_c G_d (Z_c + R_d) + Z_g G_c G_d}. \quad (2.10)$$

2.6.2 Capacitor Current Feedback

The CCF is a AD based on the capacitor current measurement with a gain of K_c , the value is summed to the control output. K_c is the tuning variable of this strategy. Fig. 7 shows the block diagram for this strategy.

The transfer functions for the grid and converter current feedback are:

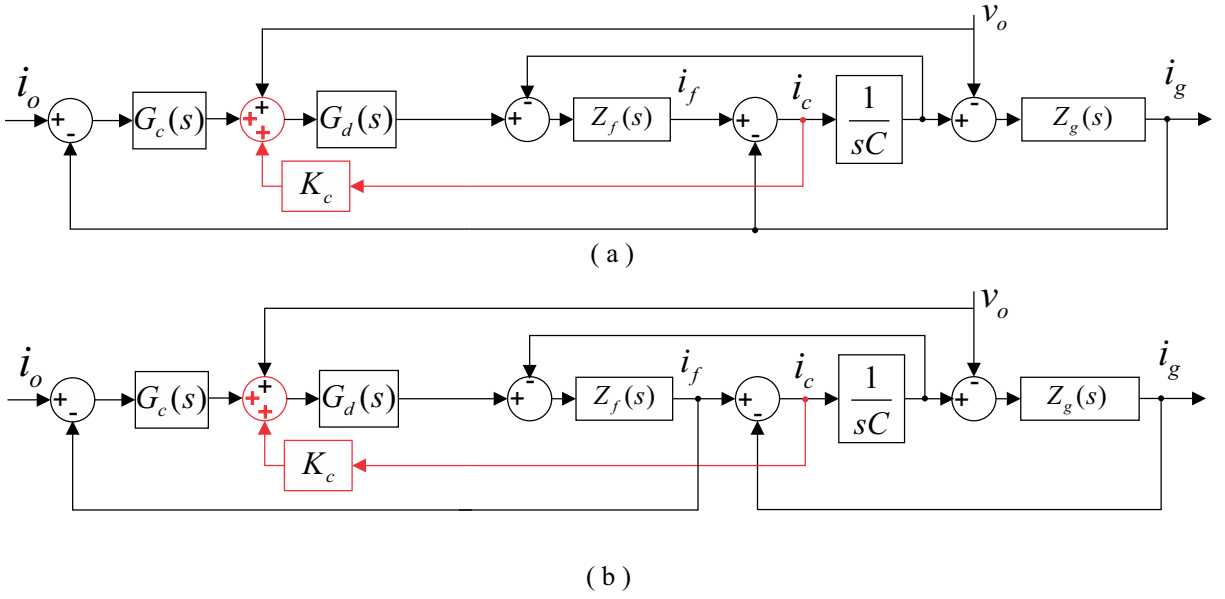


Figura 7 – Diagram of the average model for the system with CCF for the: (a) grid current feedback and (b) converter current feedback. The feedback implementation is represented in red.

$$Z_{og}(s) = \frac{Z_f + Z_c - G_d Z_c - K_c G_d}{Z_f Z_g + Z_c Z_g + Z_c Z_f + G_c G_d Z_c - K_c G_d Z_g}, \quad (2.11)$$

$$Z_{of}(s) = \frac{Z_f + Z_c - G_d Z_c + G_c G_d - K_c G_d}{Z_f Z_g + Z_c Z_g + Z_c Z_f + G_c G_d Z_c + Z_g G_c G_d - K_c G_d Z_g}. \quad (2.12)$$

2.6.3 Capacitor Voltage Feedback

The CVF function similarly to that of the CCF, but instead of using the capacitor current, it measures the capacitor voltage. This value passes by a filter with derivative characteristics in a frequency bandwidth. The filter transfer function is presented as follows:

$$L(s) = K_v C \omega_{max} \frac{s + K_f \omega_{max}}{s K_f + \omega_{max}}, \quad (2.13)$$

where K_v is an adjusting constant, ω_{max} is the frequency where the filter reaches the maximum phase, and K_f is given by:

$$K_f = \sqrt{\frac{1 - \sin(\phi_{max})}{1 + \sin(\phi_{max})}}, \quad (2.14)$$

where ϕ_{max} is the filter maximum phase. Furthermore, Fig. 8 shows the system block diagram.

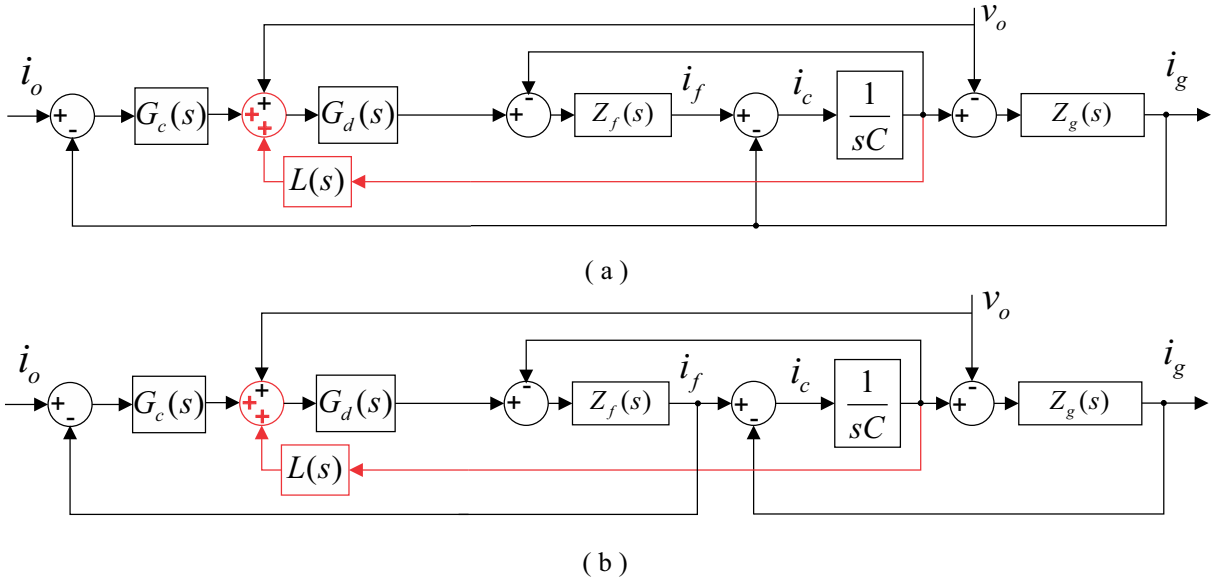


Figure 8 – Diagram of the average model for the system with CVF for the: (a) grid current feedback and (b) converter current feedback. The feedback with the filter implementation is represented in red.

The resulting inverter output impedance for the grid and converter feedback are:

$$Z_{og}(s) = \frac{Z_f + Z_c - G_d Z_c - L Z_c G_d}{Z_f Z_g + Z_c Z_g + Z_c Z_f + G_c G_d Z_c - L Z_c G_d Z_g}, \quad (2.15)$$

$$Z_{of}(s) = \frac{Z_f + Z_c - G_d Z_c + G_c G_d - L Z_c G_d}{Z_f Z_g + Z_c Z_g + Z_c Z_f + G_c G_d Z_c + Z_g G_c G_d - L Z_c G_d Z_g}. \quad (2.16)$$

2.6.4 Notch Filter

In this strategy, a notch filter is implemented in the current control output and adjusted to the resonance frequency of the LCL filter, eliminating any undesired oscillation. The notch transfer function is:

$$N(s) = \frac{s^2 + \omega_m}{s^2 + 2Q\omega_m + \omega_m}, \quad (2.17)$$

where ω_m is the cutoff frequency, and Q is the term used for tuning the damp. Fig. 9 shows the block diagram of this implementation.

And the model of the output impedance for the grid and converter current feedback are:

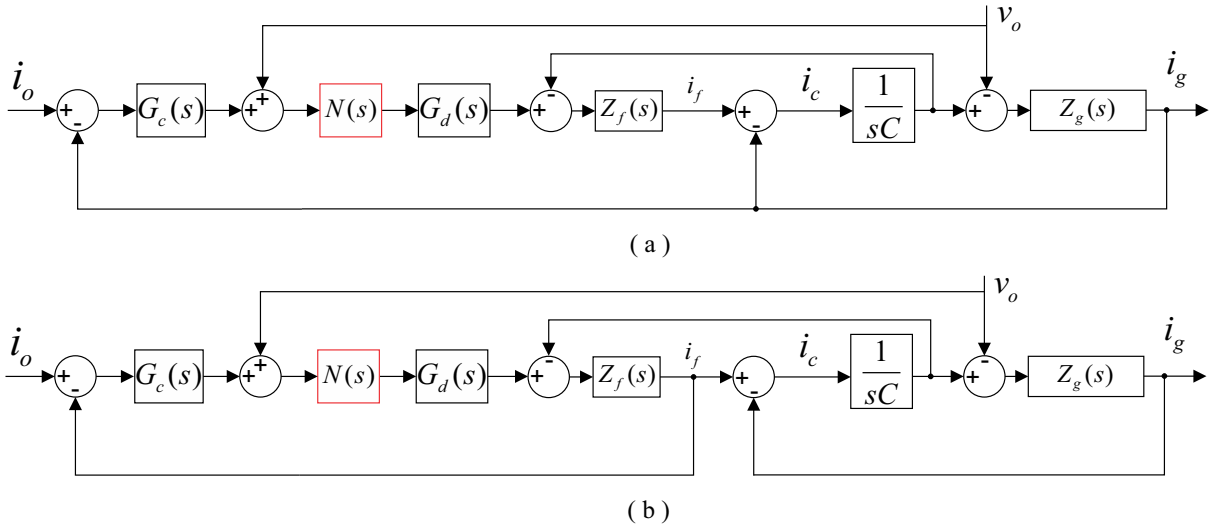


Figure 9 – Diagram of the average model for the system with NF for the: (a) grid current feedback and (b) converter current feedback. The notch filter implementation is indicated in red.

$$Z_{og}(s) = \frac{Z_f + Z_c - NG_d Z_c}{Z_f Z_g + Z_c Z_g + Z_c Z_f + NG_c G_d Z_c}, \quad (2.18)$$

$$Z_{of}(s) = \frac{Z_f + Z_c - NG_d Z_c + NG_c G_d}{Z_f Z_g + Z_c Z_g + Z_c Z_f + NG_c G_d Z_c + NZ_g G_c G_d}. \quad (2.19)$$

2.6.5 Control transfer function for the DQ and $\alpha\beta$ frames

The control frame in $\alpha\beta$ has the following control transfer function:

$$G_d(s) = K_p + \frac{K_r s}{s^2 + \omega^2}, \quad (2.20)$$

As for the PI control, the function is has follow.

$$G_d(s) = K_p + \frac{K_i}{s}. \quad (2.21)$$

However, as the PI control has a frequency shifting caused by the PLL (Pugliese; Kwon; Liserre, 2020), a compensation is necessary for the passive model to accurately represent the inverter. This shift is caused by a three-phase system that possesses a positive sequence frequency of ω_f , has its frequency shifted in the control by ω , the system

nominal frequency and the lock frequency of the PLL, resulting in a control frequency of $\omega_f - \omega$, as the PLL displace the system frequency. As for a negative sequence, the frequency shifting adds to the control frequency, resulting in $\omega_f + \omega$ (Pugliese; Kwon; Liserre, 2020). This is exemplified by the following equation.

$$V^{+*} = V^+(\omega_f - \omega), \quad (2.22)$$

$$V^{-*} = V^-(\omega_f + \omega), \quad (2.23)$$

where V^+ and V^- is a generic measured voltage signal of frequency ω_f for the positive and negative sequence, respectively. V^{+*} is the resulting positive sequence voltage signal, with frequency of $(\omega_f - \omega)$, in the control. And V^{-*} is the negative sequence voltage signal in the control, with frequency $(\omega_f + \omega)$.

This effect causes changes in the control function of the system, to be able to represent the output of the system, the frequency shifting needs to be compensated (Wang; Harnefors; Blaabjerg, 2018). Therefore, the resulting control transfers functions for the passive model are:

$$G_{d+}(s) = K_p + \frac{K_i}{s - j\omega}, \quad (2.24)$$

$$G_{d-}(s) = K_p + \frac{K_i}{s + j\omega}. \quad (2.25)$$

Other effects that the PLL may cause in the system, although those can be disregarded if a PLL attenuates frequencies in its output other than the nominal frequency of the grid (Wang; Harnefors; Blaabjerg, 2018). Therefore, in this work only the frequency shifting is considered, and the proposed model performance is compared with the results of two PLL, the SRF and the DSOGI.

3 Case Study

The system parameter used in the simulations implemented in the software *plecs* are shown in Table 1.

Tabela 1 – Inverter and grid parameters employed in the simulations.

Description	Parameters	Value
Rated Power	P_n	10 kVA
Rated Voltage	V_l	380 V
Continuous voltage	V_{dc}	750 V
Rated Frequency	f_n	60 Hz
Grid inductance	L_{gg}	0.1 mH
Filter inductance	L_f and L_g	0.4084 mH
Filter capacitance	C	7.7527 μ F
Switching frequency	f_{sw}	12 kHz
Propositional gain	K_p	3.27 Ω
Resonant gain ($\alpha\beta$)	K_r	1000 Ω/s
Integral gain (DQ)	K_i	30.8 Ω/s
Reactance/Resistance	X_L/R	40

The Reactance/Resistance ratio is applied for all inductors in the system. For the filter project, a ratio of 3 is employed for the switching and filter resonance frequency.

As for the damping strategies, each of the current feedback changes the dynamic of the system, therefore, the values of each damping strategies is adjusted, the values are listed in Table 2. As for ϕ_{max} in the CVF, it's adopt a value of 75° for all situations.

Tabela 2 – Damp values of each strategy employed.

Variable	Damping Strategy			
	R_d	K_c	K_v	Q
Inverter side (I_f)	0.6 Ω/s	0.95 Ω/s	1.1 Ω/s	0.2 s^{-1}
Grid side (I_g)	2.6 Ω/s	4.2 Ω/s	2.0 Ω/s	0.8 s^{-1}

Table 3 shows the percentage of each harmonics according to the rated voltage. The selected values are individually below the requirements in PRODIST.

Fig 10 shows the behavior of the grid with the value presented in Table 3.

Tabela 3 – Percentage value of each voltage harmonic presented in the grid.

Harm.	5°	7°	11°	13°	17°	19°
Value	6.0%	5.0%	3.5%	3.0%	2.0%	1.5%

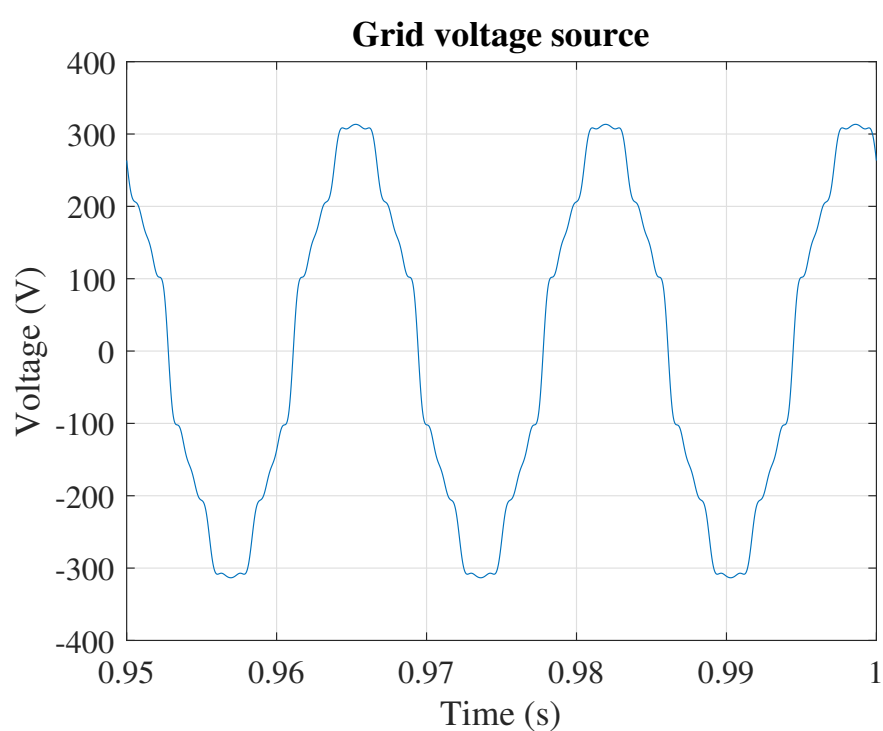


Figura 10 – Grid voltage source behavior

4 Results and Discussions

The main goal of the proposed model is to simulate the behavior of the inverter therefore, to confirm if the model is indeed representing the natural behavior of the transfer function, a bode diagram comparing the frequency response of the system transfer function and the model for different frequencies is presented in Fig. 11.

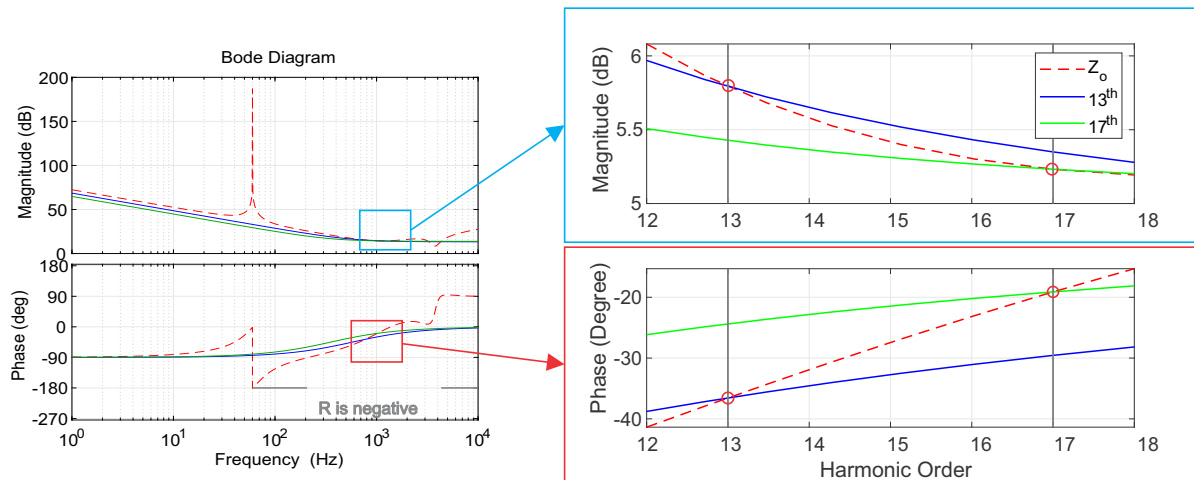


Figure 11 – Bode diagram, comparison of the output impedance of the transfer function and the Norton model for a specific frequency.

This indicates that the model represents perfectly the steady-state response of the system for a specific frequency, and only that frequency. Nonetheless, for each frequency to be represented, an RLC is required. The transfer function presents an impedance peak in the 60 Hz in this frequency, it is expected that the inverter would be the only one to inject current in the grid. With a high impedance value, the parallel impedance in the Norton model is close to an open circuit. Therefore, the grid represented by the voltage source does not generate a current. However, the inverter represented by the current source I_o injects all the current in the grid.

Furthermore, the model is made in a passive representation, so it is stable if the real part of the impedance is positive, for the negative part, when the angle of Z_o is between 90° and 270°, the system is unstable, as shown in Fig. 11 in gray.

Figure 12 shows the system impedance for the grid in the DQ control. The general behavior of each sequence is similar to each other, the main difference is for the positive frequency in 60 Hz, where the impedance presents a peak, similarly to Fig. 11. It is important to observe that the impedance without the frequency shifting does not present a peak of impedance, this indicates that the frequency shifting for Z_{o+} correctly represents the high impedance for the 60 Hz.

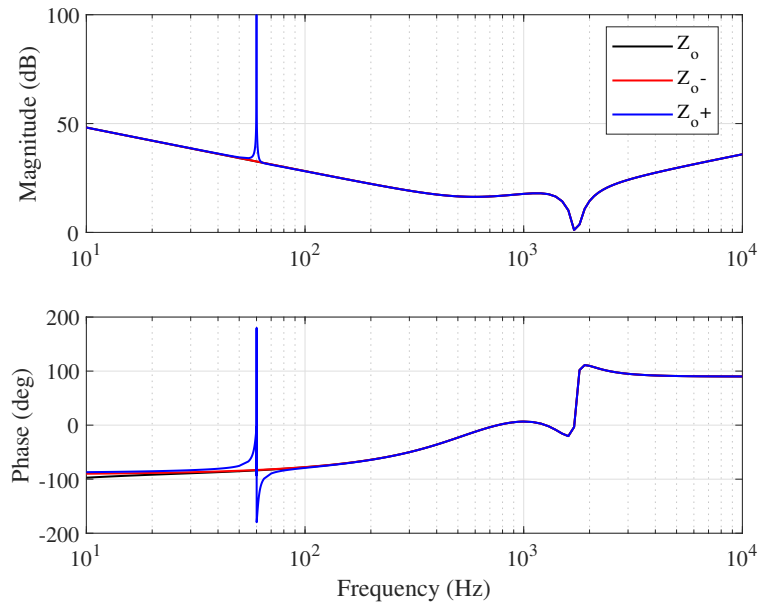


Figura 12 – Bode diagram of the output impedance for the model in DQ, where Z_o is the impedance without frequency shifting, Z_o^+ the impedance for the positive sequence and Z_o^- for the negative.

A variety of simulations were implemented that includes, each of the control strategy, with $\alpha\beta$ and dq frames, as also each current feedback, and each damping strategy. For the DQ frame, a comparison between the two of PLL, the SRF and DSOGI are presented.

For the sake of simplicity, only the results using the control with converts current feedback, and PD, are presented in function of the time, as all the other results are similar. Therefore, the results are shown in Fig. 13 and 14, where the conventional model and the proposed model based on the Norton model are presented.

In Fig. 13, it is possible to observe that the switching model presents high-order harmonics, that are derived from the switching, therefore, as in the proposed model the switching effects are disregarded, the new model lacks it. Nonetheless, the grid harmonics are represented in the model, with a comparison between them in the Fourier spectra. For the considered harmonics, there are any considerable difference.

Following the same strategy, Fig. 14 shows the comparison between the proposed model and the response of the grid current, for two PLLs. It is important to observe the possible impacts a PLL may have in the system response, and the PLL disregard. The other important observation is that the error in comparison with the SRF presents a decreasing error as the frequency increases.

It is possible to observe that the new model better represents the system with the DSOGI-PLL, then the SRF. This is due to the disregard of possible effects the PLL may have, the DSOGI has a better performance locking the grid frequency, this is due to the

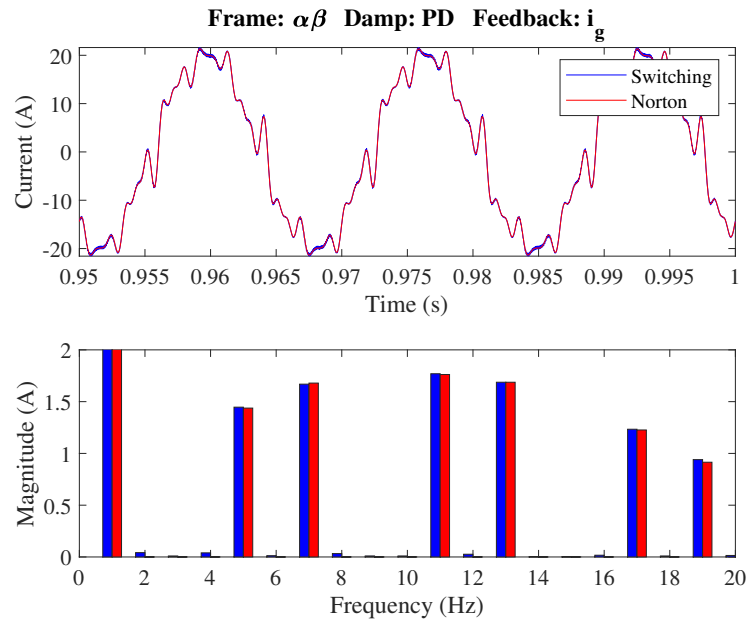


Figura 13 – Graph in time with the grid current response for the switching and proposed model, and their spectrum response with zoom in the harmonics.

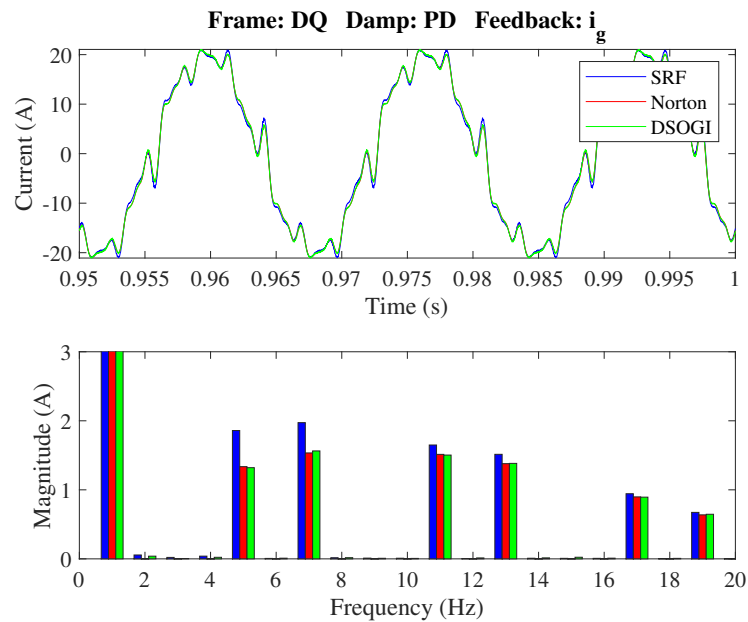


Figura 14 – Graph in time with the grid current response for the switching and proposed model, and their spectrum response with zoom in the harmonics. The results of the switching model are presented for the SRF and DSOGI PLL

better harmonic filter the strategy presents, getting closer to an ideal PLL than the SRF.

For a general comparison between the different implementations, the grid current TDD, up to the 50^o harmonic, is calculated for each situation, and presented in Table 4 and 5, respectively, for the DQ and $\alpha\beta$ axis.

Tabela 4 – Values of TDD for each of the implementation for the control in the DQ frame.

	Grid Current Feedback			Inverter Current Feedback		
	<i>Switching</i>	<i>Norton</i>		<i>Switching</i>	<i>Norton</i>	
PLL	SRF	DSOGI	-	SRF	DSOGI	-
PD	22.2%	19.1%	18.9%	18.6%	15.5%	15.4%
CCF	17.4%	14.4%	14.4%	17.5 %	14.4%	14.4%
CVF	20.0%	17.1%	17.0%	17.3%	14.6%	14.6%
NF	59.2%	54.8%	54.3%	21.5%	18.4%	18.4%

Tabela 5 – Values of TDD for each of the implementation for the control in the $\alpha\beta$ frame.

	Grid Current Feedback		Inverter Current Feedback	
	<i>Switching</i>	<i>Norton</i>	<i>Switching</i>	<i>Norton</i>
PD	21.8%	21.8%	18.2%	18.2%
CCF	16.8%	16.8%	17.0%	17.0%
CVF	20.7%	20.7%	17.6%	17.4%
NF	42.3%	42.0%	23.6%	23.6%

As it can be observed, the TDD between each implementation is very similar, only presenting a considerable difference when compared with the use of an SRF-PLL, nonetheless, this difference is can be observed in Fig. 14. The TDD indicates that the proposed model has a close harmonic response as of the switching model.

The proposed model provides a reduction in the step size of the simulation, this is possible because it disregards the switching from the semiconductors components. Fig. 15 shows the simulation time and relative error of the TDD obtained for different step sizes, the error is obtained in reference with step size of 83.333 ns. The results were obtained in a system with a PD, with grid current feedback and control in $\alpha\beta$ axis.

It is possible to implement the model in higher step sizes for the proposed model than the switching model, as it presents a TDD error around a step size of 30 μs , while the proposed model only presents a similar error around 0.3 μs .

Besides that, the proposed model can be implemented in higher step sizes than the switching model, what consequently results in a lower simulation time.

The time of each model is presented in the Tables 6 and 7, respectively, for the control in the dq and $\alpha\beta$ frames. The step size for the proposed model is 30 μs and for

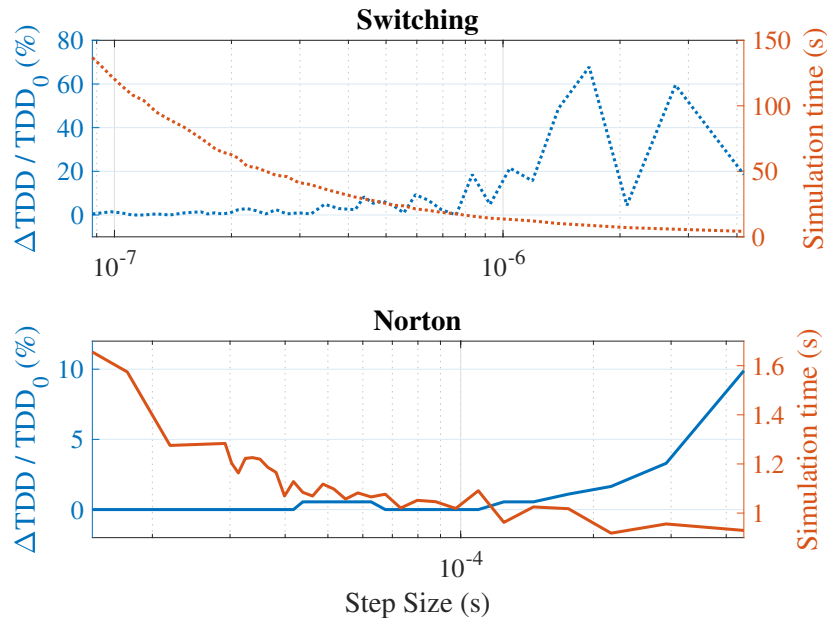


Figure 15 – Graph indicating the behavior of the TDD error and simulation time in different step size for each model.

the switching model is $0.3 \mu\text{s}$. Each situation is simulated 5 times and the average time is presented. The simulation were executed in a computer with 8GB of RAM and an processor Intel Core i7 of 8th generation.

Tabela 6 – Average time each simulation took with 5 samples in the $\alpha\beta$ frame.

	Simulation Time (s)			
	Grid Current Feedback		Inverter Current Feedback	
	<i>Switching</i>	<i>Norton</i>	<i>Switching</i>	<i>Norton</i>
<i>PD</i>	21.184	0.29102	21.332	0.30048
<i>CCF</i>	20.846	0.29472	21.234	0.30106
<i>CVF</i>	21.932	0.29186	22.415	0.29763
<i>NF</i>	22.560	0.30432	21.849	0.29377

All simulations of the proposed model presented lower time than the switching, with the times close to 0.3 s, while the model switching presents performance around 20s.

Tabela 7 – Average time each simulation took with 5 samples in the DQ frame.

	Simulation Time (s)					
	Grid Current Feedback			Inverter Current Feedback		
	<i>Switching</i>		<i>Norton</i>	<i>Switching</i>		<i>Norton</i>
	<i>PLL</i>	<i>SRF</i>	<i>DSOGI</i>	-	<i>SRF</i>	<i>DSOGI</i>
<i>PD</i>	18.366	21.163	0.31544	18.884	21.506	0.32219
<i>CCF</i>	19.312	21.942	0.30906	19.653	21.364	0.31802
<i>CVF</i>	21.414	22.120	0.31668	19.992	21.682	0.31890
<i>NF</i>	18.899	21.169	0.32314	19.710	21.360	0.31984

5 Conclusion

This work proposes an impedance model for the grid-tie inverter. From the bode diagram, the model represents the inverter output impedance for only one frequency, making necessary for individual circuits to represent each individual harmonic. Furthermore, the bode also presents an impedance peak in the 60 Hz of the grid. For the control in DQ, the requirement of a synchronous loop added a frequency shifting, observed in the bode diagram.

The models are evaluated using the TDD value, and present very similar results, where the error of TDD is lower than 1% for all situations, excluding the SRF-PLL. As for the different PLL, the DSOGI presented close results to the proposed model, as it presents a stronger lock to the grid fundamental frequency. Therefore, when compared to the SRF the proposed model lack precision, this is caused by the disregard of other PLL effects. For the DSOGI, the model is able to present similar results in comparison with the switching, therefore, the model represents well a system with a PLL that attenuates undesired oscillations.

The proposed model can be implemented in higher step sizes than the conventional switching model, consequently presenting lower simulation times, while keeping a considerable accuracy, accordingly to the TDD results.

Nonetheless, the proposed model disregards the switching effects of the system and the transient response, and each branches of the passive representations of the inverter can represent only one frequency. However, it is able to represent a more complex model only with passive components, and for a system with a strong PLL, it is able to represent it as well, doing so with a lower simulation time. Finally, the model still can be improved, with the addition of other PLL effects.

Referências

Cespedes, M.; Sun, J. Impedance modeling and analysis of grid-connected voltage-source converters. *IEEE Transactions on Power Electronics*, v. 29, n. 3, p. 1254–1261, 2014. Quoted on page 12.

Gao, F.; Gu, X.; Ma, Z.; ZHANG, C. Redistributed pulsewidth modulation of mmc battery energy storage system under submodule fault condition. *IEEE Transactions on Power Electronics*, v. 35, n. 3, p. 2284–2294, 2020. Quoted on page 12.

Gomes, C. C.; Cupertino, A. F.; Pereira, H. A. Damping techniques for grid-connected voltage source converters based on lcl filter: An overview. *Renewable and Sustainable Energy Reviews*, v. 81, p. 116–135, 2018. ISSN 1364-0321. Quoted on page 19.

Heskens, P.; Duarte, J. L. Harmonic reduction as ancillary service by inverters for distributed energy resources (der) in electricity distribution networks. In: . [S.l.: s.n.], 2007. Quoted on page 12.

Jacinto, I. A. N. *Impedance-Based Norton Model applied to Grid-Connected Photovoltaic Inverters*. 62 f. Monografia (Monografia) — Departamento de Engenharia Eletrica, Universidade Federal de Viçosa, Viçosa, Minas Gerais, 2021. Quoted 2 times on pages 7 e 14.

Li, C. Unstable operation of photovoltaic inverter from field experiences. *IEEE Transactions on Power Delivery*, v. 33, n. 2, p. 1013–1015, 2018. Quoted on page 12.

Mollerstedt, E.; Bernhardsson, B. Out of control because of harmonics-an analysis of the harmonic response of an inverter locomotive. *IEEE Control Systems Magazine*, v. 20, n. 4, p. 70–81, 2000. Quoted on page 12.

Pugliese, S.; Kwon, Y.; Liserre, M. Positive-negative sequence srf-pll model for accurate stability analysis in grid-tied converters. In: *2020 IEEE Energy Conversion Congress and Exposition (ECCE)*. [S.l.: s.n.], 2020. p. 3593–3600. Quoted 2 times on pages 23 e 24.

Puranik, I.; Zhang, L.; Qin, J. Impact of low-frequency ripple on lifetime of battery in mmc-based battery storage systems. In: *2018 IEEE Energy Conversion Congress and Exposition (ECCE)*. [S.l.: s.n.], 2018. p. 2748–2752. Quoted 3 times on pages 12, 13 e 18.

Vieto, I.; Sun, J. Small-signal impedance modelling of type-iii wind turbine. In: *2015 IEEE Power Energy Society General Meeting*. [S.l.: s.n.], 2015. p. 1–5. Quoted on page 12.

Wang, F.; Duarte, J. L.; Hendrix, M. A. M.; Ribeiro, P. F. Modeling and analysis of grid harmonic distortion impact of aggregated dg inverters. *IEEE Transactions on Power Electronics*, v. 26, n. 3, p. 786–797, 2011. Quoted 2 times on pages 12 e 17.

Wang, X.; Blaabjerg, F. Harmonic stability in power electronic-based power systems: Concept, modeling, and analysis. *IEEE Transactions on Smart Grid*, v. 10, n. 3, p. 2858–2870, 2019. Quoted 2 times on pages 12 e 14.

Wang, X.; Harnefors, L.; Blaabjerg, F. Unified impedance model of grid-connected voltage-source converters. *IEEE Transactions on Power Electronics*, v. 33, n. 2, p. 1775–1787, 2018. Quoted on page [24](#).

Wang, Y.; Chen, X.; Zhang, Y.; Chen, J.; Gong, C. Impedance influence analysis of phase-locked loops on three-phase grid-connected inverters. In: *2018 International Power Electronics Conference (IPEC-Niigata 2018 -ECCE Asia)*. [S.l.: s.n.], 2018. p. 1177–1182. Quoted on page [13](#).